A re-examination of the structure of ganophyllite

RICHARD A. EGGLETON

Geology Department, Australian National University Canberra, A.C.T., Australia

AND

STEPHEN GUGGENHEIM

Department of Geological Sciences, University of Illinois at Chicago, Chicago, Illinois 60680, USA

ABSTRACT. The superstructure of ganophyllite has been analysed using subcell single crystal X-ray data and electron-optical observations. The full cell (supercell), space group $A2/a$, $a = 16.6$, $b = 26.6$, $c = 50$ Å, $\beta = 94°$, has the approximate formula $(K,Na,Ca)_6^{+7.5}(Mg,Fe,Mn)_{24}$ $[Si_{32.5}Al_{7.5}]O_{96}(OH)_{16}21H_2O$, $Z = 8$. A structure is proposed in which triple chains of silica tetrahedra parallel to X form narrow 2:1 layers with sinusoidal Mn-octahedral sheets. The triple chains are connected laterally, and across the interlayer, by pairs of inverted tetrahedra, linking to each other into four-member rings parallel to (010). Polytypes are generated by various displacements of the inverted tetrahedra.

KEYWORDS: ganophyllite, crystal structure, superstructure.

THE manganoan layer silicate ganophyllite belongs to a group of minerals in which a relatively large octahedral sheet is co-ordinated to a smaller tetrahedral sheet. The resulting lateral misfit is accommodated in these silicates by modulations to the tetrahedral sheet. For example, the reversal and relinkage of tetrahedral apices leads to the development of a superlattice along X in antigorite (Zussman, 1954) or a superlattice within the X-Y plane in stilpnomelane (Eggleton, 1972), greenalite (Guggenheim et al., 1982) and bannisterite (Threadgold, unpublished). In each of these cases, limited tetrahedral out-of-plane tilting occurs along with curvature of the octahedral sheet to minimize further the lateral misfit of the component sheets.

The subcell of ganophyllite has been described by Kato (1980) as having layers comprising a continuous octahedral sheet and opposing triple-width silicate tetrahedral chains. These chains extend parallel to X on either side of the octahedral sheet. Alternatively, the structure may be considered a modified 2:1 layer silicate having a discontinuous tetrahedral sheet with periodic rifts along Y after every six tetrahedra, which is the silicate tetrahedral chain width. To minimize the misfit between the

tetrahedral and octahedral components, the chains are staggered across the octahedral sheet so that the rifts between chains are offset. The rift pattern allows a marked sinusoidal curvature of the octahedral sheet and of attached tetrahedra along Y. Partially occupied sites containing large cations, such as K, Ca, and Na, occur where rifts oppose each other across the interlayer and serve to connect adjacent layers.

More recently, eggletonite, the Na analogue of ganophyllite, has been described by Peacor et al. (1984). Although no superlattice reflections were observed in the original X-ray study, electron diffraction data (Guggenheim and Eggleton, 1986) show an identical superlattice to that found in ganophyllite. The examination of structural images and of the electron diffraction data prompted a reassessment of the ganophyllite structure, in order to resolve several apparent inconsistencies.

The superlattice of ganophyllite (Smith and Frondel, 1968; Jefferson, 1978) extends the subcell to $a = 3a_0 = 16.60$ Å, $b = 2b_0 = 27.13$ Å and $c = 2c_0 = 50.18$ Å. The superlattice reflections are weak relative to the subcell reflections and have a complex pattern of extinctions. Jefferson used a 'one-atom' modelling technique to show that the pattern of superlattice intensities can be explained by structural columns extended parallel to [100] and with relative displacements of $\pm a/6$. Jefferson showed that two polytypes may be derived and found diffraction evidence for each. It is likely that such $a/3$ displacements may be consistent with a triple chain structural model in which chains are translated by $a/3$ (i.e. one subcell). However, the subcell as presently known cannot account for structural variants with differing $a/3$ translations, since translations of one subcell vector produces structural congruency. Kato (1980) recognized this deficiency and suggested that the X axis superlattice results from the ordering of the interlayer cations

coupled to Al/Si tetrahedral ordering, but did not elaborate further. However, the nature of the diffuse scattering in $h \neq 3n$ reflections as described by Jefferson (1978) favours positional disorder rather than substitutional effects.

Dunn et al. (1983) provided chemical data for ganophyllite from three localities and found in each case, that the sum of octahedral and tetrahedral cations amount to 20.7 per empirical formula unit. In contrast, eggletonite (Peacor et al., 1984) sums to 21.1 and the subcell model calculates to 20, based on an octahedral to tetrahedral cation ratio of 8:12. Dunn et al. concluded that such variations in the natural material are caused by volatilization of water during electron microprobe analysis, producing a higher than expected oxide weight percent total. However, these analyses show an oxide total ($\sim 89.1\%$) consistent with the determined total water of 10.4%.

Based on the subcell model, the cohesiveness of the structure is dependent on the linkage of the layers by $K + Na + Ca$. The total interlayer charge per 12 tetrahedra is $+2$, a value between the $+1$ charge per 12 tetrahedra of smectite and $+3$ per 12 tetrahedra of the true micas. It would be anticipated that this low interlayer charge would confer little cohesion between ganophyllite layers, leading to submicaceous physical properties. In contrast, both ganophyllite and eggletonite are brittle, and have a Mohs hardness of 3 to $4\frac{1}{2}$.

The subcell model (Kato, 1980) refined to a residual value, R, of 0.078, indicated that the model is largely correct. However, the anisotropic thermal parameters for the interlayer cation site are exceedingly large; the equivalent isotropic thermal parameter is $15.7\,e^{-}/\text{Å}^{3}$. Such a high thermal parameter, even for a subcell refinement indicates the possibility of a misplaced atom.

In summary, difficulties involving the model include problems regarding (1) the development of the superlattice and polytypism, (2) chemistry, (3) the compatibility of the structure with the mineral's physical properties, and (4) the possible location of the interlayer cation. In order to resolve these inconsistencies, we have re-examined the original X-ray data, kindly made available to us by Professor T. Kato. In addition, we have combined this information with electron optical data to propose a modification to the subcell and a model for the ganophyllite superstructure.

Further refinement of the subcell

A description of the ganophyllite sample from the Harstig Mine, Pajsberg, Sweden, and experimental conditions for data collection are given by Kato (1980). Additional chemical data are given in Dunn et al. (1983). The 1490 reflections received were used initially to confirm the earlier results, but with isotropic temperature factors.

A least-squares refinement program was used to refine positional parameters only. Equivalent isotropic temperature factors $[B_{eq} = 4/3(\beta_{11}a^{*2} + \beta_{22}b^{*2} + \beta_{33}c^{*2})]$ were calculated on the basis of the reported anisotropic thermal parameters. Site multiplicity factors for partially occupied sites, based on this subcell model, were refined in alternate cycles with the isotropic parameters. Finally, site multipliers were not allowed to vary, and all positional and thermal parameters varied together. The interlayer cation (K) thermal parameter increased in size and was reset to $15.8\ e^{-1}/\text{Å}^{3}$. An electron density direct Fourier map showed no electron density at the interlayer cation site, in accord with the low occupancy indicated by the site multiplier refinement and the very high thermal parameter. The interlayer cation was removed from the refinement process, several additional cycles made, and a difference Fourier map computed. Although a 'peak' was observed at position 0.0, 0.0, 0.0, this peak was below background. Attempts to refine the thermal parameters of all atoms anisotropically, both with and without K at the origin, were only partially successful. H_2O1 and H_2O2 did not produce physically meaningful results.

Inspection of a Patterson map indicated that the Mn atoms were correctly located and successive electron density Fourier maps produced results similar to the subcell model of Kato. However, in contrast to the earlier model, small peaks were detected near $z = 0.0$ in direct Fourier maps. However, when difference Fourier maps were calculated, these peaks were not resolved. Professor Kato kindly provided an additional 360 reflections, primarily $00l$ and weak reflections, that had been removed prior to the subcell determination. With the additional data, the inconsistency was resolved and these peaks appeared in both the direct and difference Fourier maps. These results explain also why the peaks were not located in the original study, since difference Fourier maps were used exclusively in the latter stages of the structure determination. For comparison, Tables I and II present the results of the refinement for the earlier subcell model and the present one, both using the complete data set.

Two of the additional peaks observed in the Fourier maps are approximately $1\frac{1}{4}$ electrons high and are designated in Table II as O(9) and O(10). If these peaks are interpreted as partially occupied oxygen sites in the subcell, then they could represent apical oxygens of tetrahedra inverted relative to those coordinating to the octahedral sheet. If this interpretation is proper, then the partially occu-

Table I.   Results of the ganophyllite subcell structure refinements.

	Kato (1980) model		Double Atom Model (this study) Isotropic
	Anisotropic	Isotropic	
Number of reflections	1850	1850	1850
[1]R1	0.101	0.134	0.097
[2]R2	0.115	0.140	0.102
Number varied parameters	[3]152	[3]69	[4]102

1. $R_1 = \Sigma(\,||Fo| - |Fc||)/ |Fo|$

2. $R_2 = \Sigma\left[[w(|Fo| - |Fc|)^2]/ w|Fo|^2 \right]^{1/2}$, where w=1

3. Includes site multiplicities for three atoms: K, H_2O1, H_2O2 where the latter two are equivalent to T(4) and T(5)

4. Includes site multiplicities for T(2), T(2)', T(3), T(3)', T(4), T(5), O(1), O(1)', O(2), 092)', O(5), O(5)' and K

Table II.   Atomic positional, isotropic thermal and site multiplicity parameters for ganophyllite.

	Kato (1980) Model				Double Atom Model (This study)				
	x	y	z	B	[3]m	x	y	z	B
K	0.0	0.0	0.0	[2]15.8	0.27	0.273(4)	0.349(2)	0.0574(8)	4.5(4)
Mn(1)	0.9938(4)	0.0621(2)	0.23714(9)	0.67(4)	1.0	0.9937(3)	0.0620(1)	0.23714(7)	0.74(3)
Mn(2)	0.4966(5)	0.1868(2)	0.2446(1)	0.85(4)	1.0	0.4967(4)	0.1868(1)	0.24463(8)	0.96(3)
T(1)	0.7993(7)	9.4466(3)	0.1514(2)	0.74(6)	1.0	0.7993(5)	0.4463(2)	0.1513(1)	0.64(4)
T(2)	0.802(1)	0.2183(4)	0.1381(2)	1.42(8)	0.23	0.749(3)	0.218(1)	0.1355(6)	0.3(2)
T(2)'					0.80	0.816(1)	0.2183(4)	0.1388(2)	1.2(1)
T(3)	0.298(1)	0.1058(5)	0.1289(3)	2.5(1)	0.53	0.285(2)	0.1048(7)	0.1285(3)	1.0(2)
T(3)'					0.18	0.336(5)	0.108(2)	0.1298(9)	0.3(4)
[1]T(4)	-0.014(2)	0.068(1)	0.0638(5)	-0.3(2)	0.32	0.987(1)	0.0676(7)	0.0640(3)	0.4(1)
[1]T(5)	0.558(3)	0.070(1)	0.0628(6)	-0.2(2)	0.30	0.557(2)	0.0709(8)	0.0629(4)	0.7(1)
O(1)	0.544(3)	0.176(2)	0.1140(8)	3.9(4)	0.66	0.518(3)	0.176(1)	0.1168(6)	1.8(3)
O(1)'					0.43	9.610(5)	0.178(2)	0.102(1)	2.0(4)
O(2)	0.037(3)	0.168(1)	0.1124(7)	3.7(3)	0.40	0.963(5)	0.167(2)	0.102(1)	2.3(5)
O(2)'					0.71	0.062(3)	0.171(1)	0.1147(6)	2.2(3)
O(3)	0.813(2)	0.333(1)	0.1258(5)	1.6(2)	1.0	0.814(2)	0.3342(7)	0.1255(4)	1.6(1)
O(4)	0.032(2)	0.5060(9)	0.1287(5)	1.4(2)	1.0	0.033(2)	0.5069(7)	0.1293(4)	1.5(1)
O(5)	0.283(3)	0.020(1)	0.0822(6)	2.8(3)	0.40	0.268(4)	0.030(2)	0.0711(9)	0.9(3)
O(5)'					0.61	0.293(3)	0.015(1)	0.0901(7)	1.4(3)
O(6)	0.318(2)	0.068(1)	0.1927(5)	1.4(2)	1.0	0.317(2)	0.0674(7)	0.1926(3)	1.5(1)
O(7)	0.818(2)	0.1958(8)	0.1996(5)	1.1(2)	1.0	0.820(2)	0.1960(6)	0.1998(3)	1.2(1)
O(8)	0.823(2)	0.4402(9)	0.2168(4)	0.9(2)	1.0	0.823(1)	0.4411(7)	0.2168(3)	0.9(1)
O(9)					0.13	0.609	0.089	0.000	1.0
O(10)					0.13	0.891	0.091	0.003	1.0
OH	0.324(2)	0.3216(8)	0.2121(5)	1.0(2)	1.0	0.324(2)	0.3207(6)	0.2122(3)	1.1(1)

1. T(4) labelled as H_2O1 and T(5) labelled as H_2O2 by Kato (1980).

2. Constrained to the value of the equivalent isotropic temperature factor in accord with the anisotropic thermal parameters as published by Kato (1980).

3. Refined multiplicities for the Kato model: K = 0.11, H_2O1 [=T(4)] = 0.66, H_2O2 [= T(5)] = 0.62; all others assigned 1.0 in accord with the model.

pied H_2O sites of Kato (1980) can be reinterpreted as (partially occupied) tetrahedral cation sites, designated in Table II as T(4) and T(5). The refinement progressed satisfactorily when the scattering curve of Si was used for these sites. However, O(9) and O(10) could not be refined and site multiplicities and positions were determined from difference Fourier maps. Isotropic thermal parameters were arbitrarily set to 1.0 e⁻/Å³. In addition, a peak approximately $4\frac{1}{2}$ electrons high was located in the interlayer region (designated as K in Table II). The refinement converged to equal residual (R) values for models with either alkali or oxygen scattering factors at this site; the data cannot distinguish between either alkali cations or water molecules entering this site. However, there is

not sufficient scattering material located at this site to account for all the alkali present in the structure as determined by electron microprobe analysis. On the other hand, there is sufficient scattering material generally in the interlayer channels (see fig. 1) to account for additional alkali and water molecules. This suggests that the small (approximately 0.85 electrons) peak at the origin, designated by Kato (1980) as the site for the alkali cation probably does contain a small amount of alkali material. These results are consistent with the cation exchange experiments of Guggenheim and Eggleton (1986) in which it was suggested that the alkali cations and water molecules are zeolitic in nature.

For reasons given below, atoms affected by positional disorder were split into partially occupied sites. Both a triple atom model and a double atom model were considered. However, both models refined to equal residual values and the double atom model, which has fewer variables, is reported.

Density redetermination

The density for the Pajsberg, Sweden ganophyllite (Smithsonian No. B17240) specimen used by Kato (1980) was redetermined, as was ganophyllite from Franklin, N.J. (Smithsonian No. 97499). A gradient column technique with methylene iodide diluted with methyl iodide layered over methylene iodide was used, with calibration grains of calcite ($d = 2.715$), dioptase ($d = 3.278$), $BaCl_2 \cdot 2H_2O$ ($d = 3.097$), and three density glasses ($d = 2.946$, 2.874, 2.797). All grains were approximately 0.1 mm in size and could be measured to within 0.05 mm. The measured density for the Pajsberg ganophyllite specimen of 2.83 ± 0.01 g/cm3 is in good agreement with Smith and Frondel (1968), but at odds with Dunn et al. (1983). The measured density of Franklin ganophyllite is 2.810 ± 0.01, a value unchanged after heating to 35 °C in vacuum for $1\frac{1}{2}$ hours.

Discussion

Subcell. It should be noted that a subcell structure is an average of the true structure, with atoms of the subcell often showing positional disorder. Describing excessive positional disorder in terms of thermal motion is usually not effective. We have attempted to approximate this disorder by a double-atom model, but doing so makes R value comparisons to the earlier model difficult. The much reduced R value (Table I) with fewer varied parameters is probably a function of the more realistic approach to describing positional disorder, in addition to the re-interpretation of layer connectivity. Although a low R value is important, a model must be judged on how successfully it resolves the inconsistencies noted in the introduction.

The electron density of the new subcell model presented here differs only slightly from the earlier model; three additional peaks amounting to a total in scattering material of 7 electrons are reported. However, the topology of the tetrahedral arrangement has markedly changed. Most importantly, the tetrahedral chains or strips are connected across the interlayer region by inverted tetrahedral apices. Tetrahedral connectivity across the interlayer would be expected to increase the cohesiveness of the structure and this explains the brittle nature of ganophyllite. These inversions do not occur periodically in the subcell and therefore, suggest also the origin of the superlattice.

The least-squares refinement of the site multiplicities of the tetrahedral cations indicated that the total occupancy of $T(3)$ and $T(3)'$, the tetrahedral cation site located at the edges of the tetrahedral chain or strip, is 0.71. This low total is significant since it suggests that the $T(3)$ tetrahedron reverses systematically when tetrahedral connectivity across the interlayer occurs. The site multiplicities of $T(4)$ and $T(5)$, 0.32 and 0.30, suggest that one silicon is being supplied by $T(3)$ and the other may be considered 'excess'.

The site multiplicities determined for the oxygen atoms involved in layer connectivity, O(9) and O(10), are at odds with those determined for the tetrahedral cations $T(4)$ and $T(5)$; both sets of multiplicities should be similar. However, we emphasize that the superlattice reflections are not included in the data set. These reflections contain detailed information regarding the interlayer connectivity. The inability to refine the positional coordinates of O(9) and O(10) by least-squares is related also to the use of an incomplete data set.

The $0kl$ direct Fourier projection (fig. 1) offers considerable advantages over the least-squares refinement. The $0kl$ net does not contain superlattice reflections and therefore the electron density projection presents a more realistic representation of the structure without aberrations caused by an incomplete data set. The peak heights have intensified for O(9)+O(10). When compared with other oxygen atoms, such as O(3), the peak height for O(9)+O(10) represents a multiplicity factor of 0.72, or 0.36 for each. This value compares well with the values of 0.30 and 0.32 for $T(4)$ and $T(5)$. Furthermore, the $0kl$ projection shows an additional position for the alkali and water molecules at $y = 0.166$, $z = 0.5$. However, electron density in the interlayer is sufficiently diffuse that alkali positions cannot be located precisely.
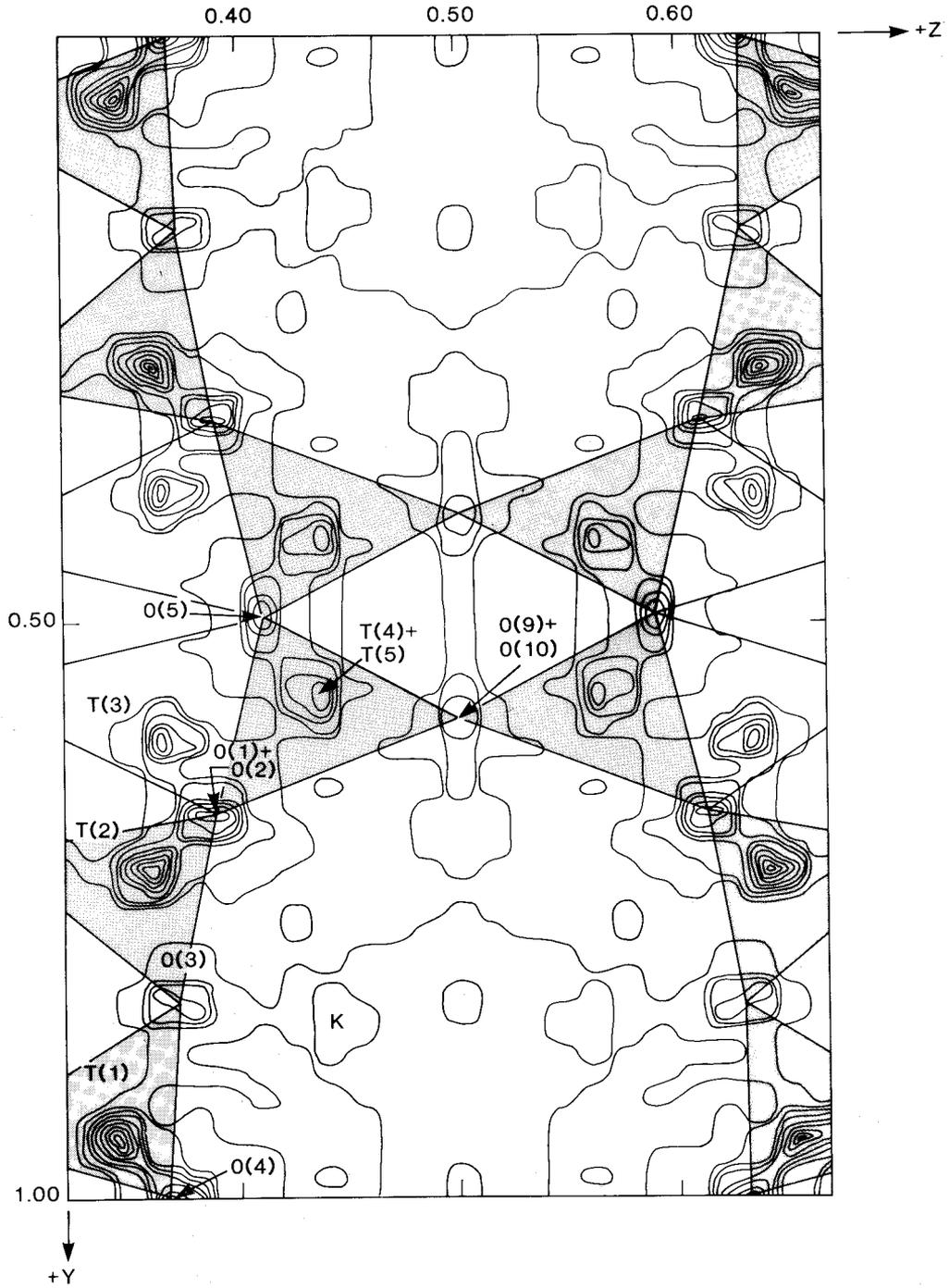
FIG. 1. 0kl Fourier synthesis. Shaded portions indicate the tetrahedral linkages proposed in the portion of the superstructure that has tetrahedral connections across the interlayer region.
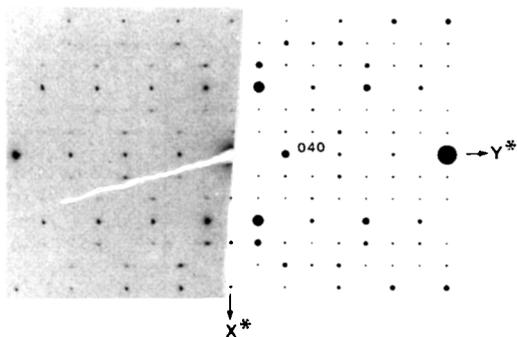
FIG. 2. $hk0$ electron diffraction pattern from Franklin ganophyllite (left), and the weighted reciprocal lattice for monoclinic ganophyllite (right). (Circle diameters proportional to $|F|$.)

In developing a model for the superstructure, we have attempted to use the positions of the split atoms in the substructure to suggest structural modifications for the superstructure. However,

because the split atom model is only an approximation for describing position disorder, we have not constrained our supercell model to precisely conform to the refined coordinates of the split atoms.

Superstructure. The major structural difference between the subcell and supercell structures of ganophyllite is attributed to the modulation that produces the threefold increase in the subcell a axis, rather than the doubling of b and c. The latter dimensional increases are detected only by the analysis of systematic (space group and non-space group) absences. In contrast, the threefold increase in a occurs in all reciprocal lattice zones other than $0kl$, with all such zones having prominent rows with $h \neq 3n$ (fig. 2). The subcell refinement suggests that the tetrahedral site occupancies may be an important factor in producing the superlattice a dimension; $T(3)$ contains about $\frac{2}{3}$ Si, $T(4)$ and $T(5)$ about $\frac{1}{3}$ each. Accordingly, the superstructure model is derived from three subcells along X, with one $T(3)$ deleted every three subcells and one $T(4)$ and one $T(5)$ added in accordance with the supercell a-glide symmetry (figs. 3 and 4). This model has
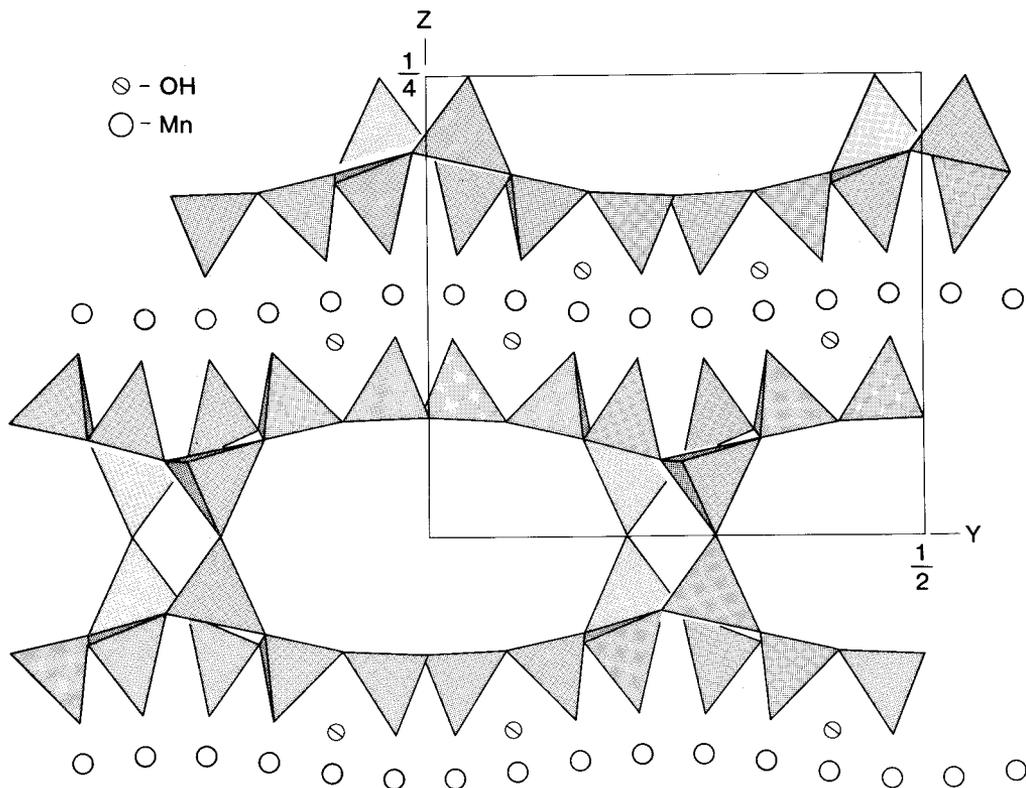

FIG. 3. The model structure of ganophyllite projected parallel to X.

triple tetrahedral chains connected laterally by inverted tetrahedra which produces fivefold and sevenfold rings of tetrahedra at the junction. Adjacent triple chains may be displaced by $a/3$, which leads to various layer geometries (fig. 4). It is most common, however, to have the triple-chains displaced in a random or semi-random arrangement to produce the streaking of $h \neq 3n$ rows in reciprocal space (fig. 2).

Jefferson (1979) described the polytypism of ganophyllite, using as a model structural rods parallel to [100] having displacements on (011) and (011) of integral multiples of $a/6$, $b/4$, $c/4$. In the real structure, the triple tetrahedral chains provide the rod-like elements. Within a single tetrahedral sheet, adjacent triple chains can only connect to each other if displacements between them are 0, or $\pm a/3$ (i.e. an integral number of subcells). Across the octahedral layer, the curving of the tetrahedral strip requires that the opposing tetrahedra be displaced by half the strip width, or $b/4$. Connectivity between octahedral and tetrahedral sheets restricts X-axis displacements to integral multiples of $a/6$ (subcell $\pm a/2$). The ganophyllite layer, 12.5 Å thick, determines the third displacement component, $c/4$, and Jefferson's equipoint vector $(\frac{1}{6}, \frac{1}{4}, \frac{1}{4})$ (printed as $(\frac{1}{4}, \frac{1}{4}, \frac{1}{6})$ on p. 495) referred to the monoclinic cell, is seen to be a result of restrictions inherent to the structure. Jefferson's interpretation of the diffraction data shows that in the monoclinic polytype two differently connected tetrahedral sheets alternate along the Z-axis. At $z = 0$ and $\frac{1}{2}$, the tetrahedral triple chains connect with no lateral (parallel to x) displacement (fig. 4a). At $z = \frac{1}{4}, \frac{3}{4}$, alternate triple chains are displaced by $a/3$ (fig. 4b).

The supercell X-ray reflections are very weak, and do not allow critical testing of this model. However, electron diffraction intensities can provide a qualitative test, and fig. 2 shows a comparison between $hk0$ electron diffraction, and the weighted reciprocal lattice calculated from a model of the supercell, repeated to conform with Jefferson's stacking sequence. The agreement between model and observed superlattice reflections is good. (The reflections 100 and 500, forbidden in space group $A2/a$, are interpreted as arising from double diffraction, a common effect in electron diffraction, particularly when the crystal is not exactly aligned. Cleavage flakes of ganophyllite are never perfectly flat, and some part of any crystal will always be slightly misoriented. Many of the strong $hk0$ reflections have adjacent strong superlattice reflections at $(h \pm 1)k0$, e.g. 320, 420. The apparent reflection 100 could be excited by double diffraction via 320 and 420, and 500 from 540 and 040. Examination of the $hk0$ diffraction patterns from very thin crystals reveals no intensity at 100 and 500, suggesting that

these reflections found from thicker crystals are indeed the products of double diffraction. The $h0l$ reciprocal lattice shows systematic absences for $l = 2n + 1$ (A-lattice), and $h = 2n + 1$ (a-glide) consistent with the space group $A2/a$.)

As explained by Kato, the curvature of the triple chains of tetrahedra, and their unusual connections parallel to Y arises from the misfit between octahedral and tetrahedral parts of the structure. The extra tetrahedra in our model help to relieve the misfit in the Y direction, as well as lengthening the two lateral chains of the triple-chain parallel to X. Although the refinement of the subcell did not reveal the location of Al in the structure on the basis of scattering power, the $T(1)$ site is sufficiently large to concentrate most of the Al in the central continuous chain of the triple-chain. There is sufficient Al in the formula to occupy at least half of the $T(1)$ site. Using the basal oxygen interatomic distances for the Si and Al tetrahedra in margarite, (Guggenheim and Bailey, 1975), a six-member straight tetrahedral [AlSi] chain has a length (spanning three subcells) of 16.5 Å, equal to the a axis of ganophyllite. The position of the interlayer cation, found by Fourier methods to lie above the tetrahedral rings involving $T(1)$, lends support to this interpretation, as it locates the interlayer cation near the Al tetrahedra, which have undersaturated basal oxygens.

Cell content. The subcell composition of this structure based on the refined occupancies is $K_{0.3}(Mn,etc.)_8(Si,Al)_{13.33}$; the supercell formula thus becomes three times this: $(K,Na,Ca)(Mn)_{24}(Si,Al)_{40}(O,OH)_{120}$. The model does not indicate the number of interlayer cations, but as no Al appears in the octahedral sites, the total interlayer change must equal the tetrahedral Al. The model formula, based on the tetrahedral sheet of fig. 4a, is $(K,Na,Ca)^{+x}Mn_{24}(Si_{40-x}Al_x)O_{96}(OH)_{16}$.

Structural formulae may be calculated using the determined oxide weight percent, measured cell volume and density only. The cell parameters as given by Kato (1980, Table I) for the Franklin and Pajsberg ganophyllites (Nos. 1 and 5) were used, but with $a = 3a_0$. The chemical composition was obtained from Dunn et al. (1983) and the density values are those given above. The predicted tetrahedral to octahedral ratio based on the model presented here is 80:48. Both the Franklin and Pajsberg ganophyllites are in close agreement with the predicted values; the Franklin ganophyllite has a ratio of 78.7:47.1 and the Pajsberg ganophyllite ratio is 79.0:48.1 (Table II).

According to Dunn et al., ganophyllite loses 7.5 wt. % H_2O on heating to 190 °C, which is 69% of the analytical H_2O. The model requires that 16 of the empirically determined 58 hydrogens be bonded
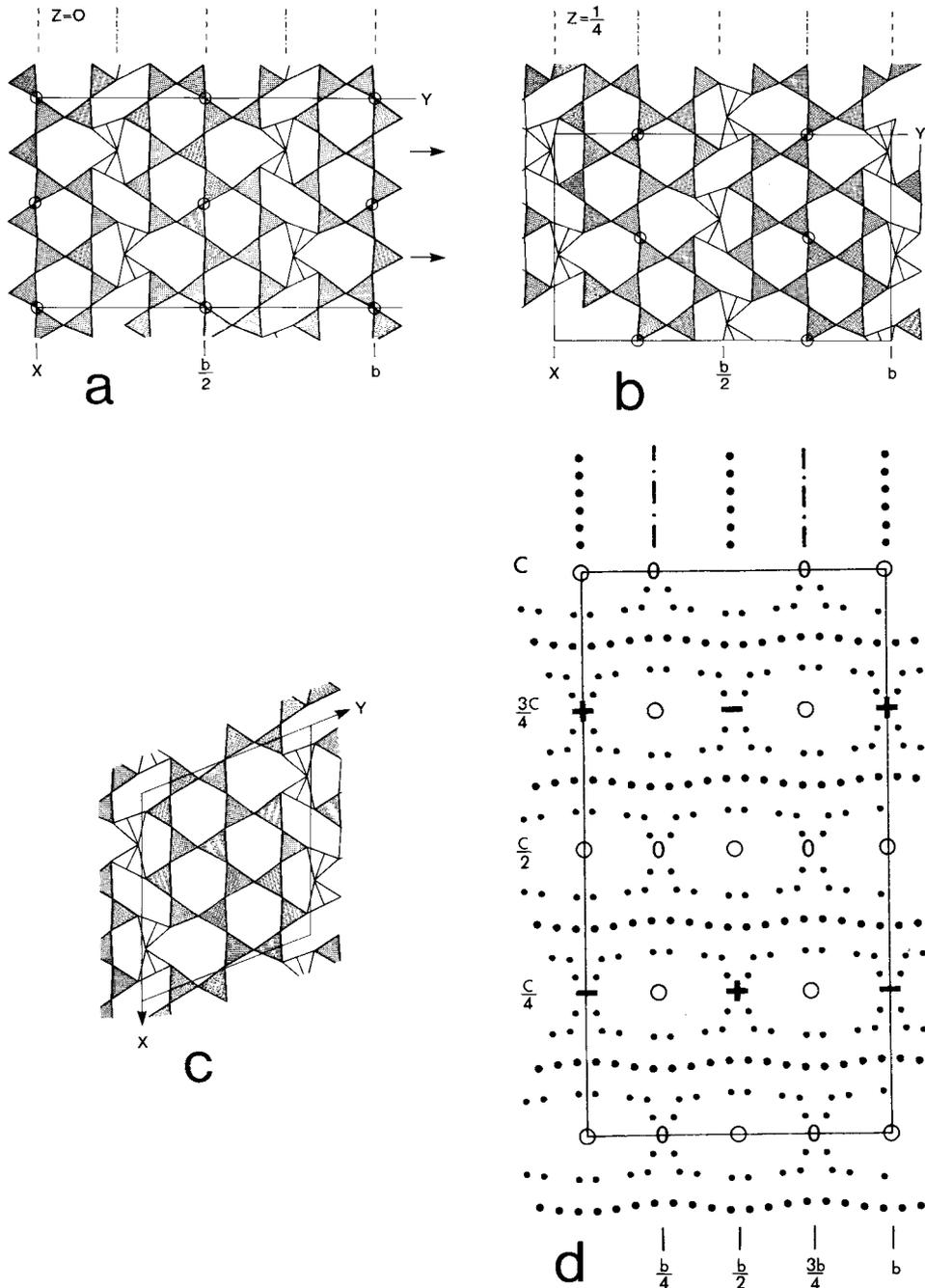
FIG. 4. Tetrahedral linkages in ganophyllite. (a) Linkage at $z = 0$, monoclinic polytype. (b) Linkage at $z = \frac{1}{4}$, monoclinic polytype. (c) Proposed triclinic linkage. Note that in the monoclinic polytype, inverted tetrahedra at $z = \frac{1}{4}$ are displaced ($\pm\frac{1}{6}, \frac{1}{4}, \frac{1}{4}$) relative to those at $z = 0$. (d) X-axis projection of the monoclinic polytype. 0, +, − refer to $a/6$ displacements of the tetrahedra connecting the triple chains. Large dots: Mn, smaller dots: Si. $A2/a$ symmetry elements are also shown.

as structural OH, leaving 72% of the hydrogens to be allocated as H_2O, again in agreement with observation.

An approximate supercell formula for Pajsberg and Franklin ganophyllites is $(K,Na,Ca)_6^{+7.5}(Mg, Fe,Mn)_{24}[Si_{32.5}Al_{7.5}]O_{96}(OH)_{16}21H_2O$ and, although the tetrahedral cation totals of Table III are low by about 1%, this deviation is well within the experimental errors for density and cell volume. The empirical cell content thus fits the proposed ganophyllite model extremely closely.

TABLE III. EMPIRICAL STRUCTURAL FORMULAE FOR GANOPHYLLITE

	Pajsberg		Franklin	
Si	32.1		32.2	
Al	7.5		7.4	
Mn	23.0		23.0	
Fe	0.3		0.2	
Zn	0.1	24.0	0.5	23.8
Mg	0.6		0.3	
Ca	0.8		1.3	
Na	2.0		1.7	
K	3.3		2.6	
H	58		58	
V	5638		5644	
D	2.83		2.81	

Chemical analyses and cell volume from Dunn et al., 1983; density this study.

Conclusion

A new type of silica tetrahedral sheet is proposed for ganophyllite. Triple chains parallel to X are linked by double pairs of inverted tetrahedra forming four-rings parallel to (010). The inverted tetrahedra link to the triple chains in five- and seven-member rings. The tetrahedral inversions produce a superlattice along X three times the subcell a dimension; regular stacking of the layers, involving $(a/6, b/4, c/4)$ displacements of the inverted tetrahedra, doubles both b and c of the subcell. The stronger tetrahedral bonding across the interlayer region compared to the K–O bonds in mica increases the hardness of ganophyllite to almost 4; the interlayer K and Na is exchangeable. The composition is (much simplified) approximately $K_6Mn_{24}(Si,Al)_{40}O_{96}(OH)_{16} \cdot 21H_2O$.

REFERENCES

Dunn, P. J., Peacor, D. R., Nelen, J. E., and Ramik, R. A. (1983) *Mineral. Mag.* **47**, 563–6.
Eggleton, R. A. (1972) Ibid. **38**, 693–711.
Guggenheim, S., and Bailey, S. W. (1975) *Am. Mineral.* **60**, 1023–9.
—— and Eggleton, R. A. (1986) *Mineral. Mag.* (in press).
—— Bailey, S. W., Eggleton, R. A., and Wilkes, P. (1982) *Can. Mineral.* **20**, 1–18.
Jefferson, D. A. (1978) *Acta Crystallogr.* **A34**, 491–7.
Kato, T. (1980) *Mineral. J. (Japan),* **10**, 1–13.
Peacor, D. R., Dunn, P. J., and Simmons, W. B. (1984) *Mineral. Mag.* **48**, 93–6.
Smith, M. L., and Frondel, C. (1968) Ibid. **36**, 893–913.
Zussman, J. (1954) Ibid. **30**, 498–512.